

RESEARCH

Open Access



Mast cells promote choroidal neovascularization in a model of age-related macular degeneration

Rabah Dabouz^{1,2*}, Pénélope Abram^{2,3}, Jose Carlos Rivera^{4,5} and Sylvain Chemtob^{1,2,5*}

Abstract

'Wet' age-related macular degeneration (AMD) is characterized by pathologic choroidal neovascularization (CNV) that destroys central vision. Abundant evidence points to inflammation and immune cell dysfunction in the progression of CNV in AMD. Mast cells are resident immune cells that control the inflammatory response. Mast cells accumulate and degranulate in the choroid of patients with AMD, suggesting they play a role in CNV. Activated mast cells secrete various biologically active mediators, including inflammatory cytokines and proteolytic enzymes such as tryptase. We investigated the role of mast cells in AMD using a model of CNV. Conditioned media from activated mast cells exerts proangiogenic effects on choroidal endothelial cells and choroidal explants. Laser-induced CNV in vivo was markedly attenuated in mice genetically depleted of mast cells ($Kit^{W-sh/W-sh}$) and in wild-type mice treated with mast cell stabilizer, ketotifen fumarate. Tryptase was found to elicit pronounced choroidal endothelial cell sprouting, migration and tubulogenesis; while tryptase inhibition diminished CNV. Transcriptomic analysis of laser-treated RPE/choroid complex revealed collagen catabolism and extracellular matrix (ECM) reorganization as significant events correlated in clusters of mast cell activation. Consistent with these analyses, compared to wildtype mice choroids of laser-treated mast cell-deficient mice displayed less ECM remodelling evaluated using collagen hybridizing peptide tissue binding. Findings herein provide strong support for mast cells as key players in the progression of pathologic choroidal angiogenesis and as potential therapeutic targets to prevent pathological neovascularization in 'wet' AMD.

Keywords Retinal degeneration, Choroidal neovascularization, Mast cells, Angiogenesis, Laser

*Correspondence:

Rabah Dabouz
rabah.dabouz@mail.mcgill.ca

Sylvain Chemtob
sylvain.chemtob@umontreal.ca

¹Department of Pharmacology and Therapeutics, McGill University, Montreal, QC, Canada

²Department of Ophthalmology, Maisonneuve-Rosemont Hospital Research Centre, Montreal, QC, Canada

³Department of Pharmacology, University of Montreal, Montreal, QC, Canada

⁴CHU-Sainte Justine Research Center, Montreal, QC, Canada

⁵Department of Ophthalmology, University of Montreal, Montreal, QC, Canada

Introduction

Choroidal neovascularization (CNV) is a pathological manifestation that involves the abnormal growth of blood vessels from the choroid through the Bruch's membrane extending into the subretinal and outer retinal space [1]. CNV is a leading cause of severe vision loss and is frequently linked with ocular disorders, notably age-related macular degeneration (AMD) [2]. While anti-vascular endothelial growth factor (VEGF) therapy has shown success in improving vision [3], it carries risks and drawbacks. A notable concern is that some patients might develop geographic atrophy as a response to the



© The Author(s) 2024. **Open Access** This article is licensed under a Creative Commons Attribution-NonCommercial-NoDerivatives 4.0 International License, which permits any non-commercial use, sharing, distribution and reproduction in any medium or format, as long as you give appropriate credit to the original author(s) and the source, provide a link to the Creative Commons licence, and indicate if you modified the licensed material. You do not have permission under this licence to share adapted material derived from this article or parts of it. The images or other third party material in this article are included in the article's Creative Commons licence, unless indicated otherwise in a credit line to the material. If material is not included in the article's Creative Commons licence and your intended use is not permitted by statutory regulation or exceeds the permitted use, you will need to obtain permission directly from the copyright holder. To view a copy of this licence, visit <http://creativecommons.org/licenses/by-nc-nd/4.0/>.

anti-VEGF treatment [4, 5], and there is still potential progression to fibrotic scars [6]. Hence, the search for new therapeutic modalities remains significant.

The role of inflammation and particularly mononuclear phagocytes in the pathogenesis of CNV has been a topic of great interest for several decades. Mast cells are tissue-resident immune cells that play a significant role in defense against pathogens and diseases [7]. They are prevalent in vascularized tissues and in locations directly exposed to external environments [8]. Upon activation, mast cells release a spectrum of pre-stored or *de novo* generated mediators. These include biogenic amines, an array of serine and other proteases, lysosomal enzymes, cytokines, chemokines, growth factors, and lipid mediators [9–11]. Mast cells are commonly linked to conditions like asthma, allergies, and anaphylaxis [12], but their role goes beyond these illnesses. These cells play a fundamental role in the immune system, with their evolutionarily preserved ability to act as first responders in recognizing pathogens and signs of infection contributing to both innate and adaptive immune responses [13]. There is increasing evidence that mast cells influence a wide spectrum of diseases, such as mastocytosis, chronic pain, cancer, cardiovascular, and neurodegenerative diseases [14–17]. In the eye, mast cells have been observed in varying amounts in the uvea, displaying a specific distribution pattern in the choroid, sclera, ciliary body, and iris [18–20]. Importantly, there is a marked increase in mast cell numbers and degranulation in the choroid in vasoproliferative AMD [21], but the mechanisms implicated in the development of CNV remain poorly characterized. In the present study, we investigated the contribution of mast cells to CNV.

Materials and methods

Animals

All animal experiments were approved by the Maison-neuve Rosemont Hospital Animal Care Committee and were performed in accordance with the Association for Research in Vision and Ophthalmology Statement for the Use of Animals in Ophthalmic and Visual Research. Adult C57BL/6J and Kit^{W^{-sh}/W^{-sh}} (Stock #030764) mice aged 10–12 weeks were purchased from Jackson Laboratory; these mice do not harbor rd1 or rd8 mutations. Mice were housed and maintained at local animal facilities under a 12-h light/dark cycle (100–200 lx) with water and normal diet food available ad libitum.

Laser-induced CNV

Male and female mice were anesthetized with a mix of ketamine (100 mg/kg) and xylazine (20 mg/kg). Corneas were anesthetized with proxymetacaine hydrochloride (0.5% Alcaine; Alcon, Fort Worth, TX, USA) and pupils dilated with 0.5% atropine (Alcon, Fort Worth, TX, USA).

Argon laser photocoagulation (50 μ m, 400 mW, 0.05 s) was utilized to rupture the Bruch's membrane at four locations per eye around the optic nerve. Mice were randomly grouped to receive intraperitoneal injections of ketotifen fumarate (25 mg/kg), tryptase inhibitor APC 366 (5 mg/kg), or vehicle. Ketotifen was administered starting 48 h before the laser burn and continued daily until the day before sacrifice. APC 366 was administered starting on the day of the laser burn and continued daily until sacrifice. Eyes were enucleated at different time points after laser photocoagulation.

Fundus fluorescein angiography

Fluorescein angiography was performed using a Micron IV scanning laser ophthalmoscope (Phoenix Laboratories, Pleasanton, CA, USA). Pupils were dilated with 0.5% atropine (Alcon, Fort Worth, TX, USA) and mice were euthanized. Fluorescein (Alcon) was administered intraperitoneally at 1 unit/gram of body weight using a 5% dilution in 0.9% sodium chloride solution. Images were taken 5 min later. A computer-assisted method was used to quantify fluorescence intensity using ImageJ software. The intensity of basal level of fluorescence in nonleakage areas was used as background fluorescence. After deduction of background signals, the total intensity of fluorescence contributed by the leaked fluorescein was used to represent the leakage. Mice injected with fluorescein were not further processed for imaging using the green channel.

Immunohistochemistry

Eyes were fixed in 4% paraformaldehyde (PFA) for 1 h and then rinsed twice with phosphate-buffered saline (PBS). The neuroretina was carefully separated from the retinal pigmented epithelium (RPE)/choroid/sclera complex which was processed for staining. The RPE/choroid complex was incubated at room temperature for 1 h with a blocking solution consisting of 1% bovine serum albumin (BSA), 1% normal goat serum, 0.1% Triton X-100, and 0.05% Tween-20 in PBS. The RPE/choroid complex was then stained with 1:100 FITC-labeled isolectin (Vector Lab; FL-1201), rhodamine-labeled isolectin (Vector Lab; #RL-1102), 1:200 rhodamine phalloidin (Cedarlane Laboratories), 1:100 tryptase (ThermoFisher: #PA5-119480), or 1:400 fluorescein-conjugated avidin D (Vector Lab; #A-2001-5) overnight. The next day, they were washed thrice then stained with the secondary antibody. Cell nuclei were stained with 4',6-diamidino-2-phenylindole (DAPI) (1:5000; Sigma-Aldrich). Flat mounts were examined using the same settings with a laser scanning confocal microscope (Leica Stellaris 8), across all experiments.

Isolation of peritoneal mast cells

Peritoneal mast cells (PMCs) were isolated from 8-week-old C57 mice. 3 mL of cold PBS and 2 mL of air were injected into the peritoneal cavity using a 27-gauge needle. After a 2-minute gentle massage, the fluid was collected using a 25-gauge needle, avoiding blood contamination. Cells were isolated by centrifugation (500 g for 5 min) and resuspended in Roswell Park Memorial Institute (RPMI) 1640 medium (A1049101, Thermo Fisher) with glutamine, interleukin (IL)-3 (10 ng/mL), stem cell factor (30 ng/mL), 10% fetal bovine serum (FBS), and 1% penicillin/streptomycin. The medium was renewed every 2 days for 1 week. PMCs were immunophenotyped by flow cytometry for CD117 and FcεR-1α using a BD LSRFortessa X-20 and analyzed with FlowJo software (Supp Fig. 1A). PMCs were treated or not with compound 48/80 (20 μM) for 30 min. The culture medium was centrifuged, and the supernatant served as conditioned media.

Isolation of bone marrow-derived mast cells

Bone marrow-derived mast cells (BMDMCs) were harvested from 8-week-old C57BL/6 mice, euthanized via cervical dislocation. Bone marrow cells were flushed from the femurs and tibias using RPMI 1640, centrifuged at 1200 rpm for 5 min at room temperature, and resuspended in RPMI 1640 supplemented with 2 mM L-glutamine, 0.07% β-mercaptoethanol, 10 mM HEPES, 10% fetal calf serum (Wisent Bioproducts #085–150), 1% antibiotics (penicillin and streptomycin), and 30 ng/mL of recombinant mouse IL-3 (R&D Systems #403-ML). The cell suspension was strained through 40 μm sterile filters (Corning #352340) and cultured in petri dishes at 37 °C with 5% CO₂ in a humidified incubator. The medium was refreshed biweekly through gentle centrifugation. Six weeks later, BMDMCs were fully differentiated, and their purity was determined by flow cytometry for CD117 (Biolegend; #105827) and FcεR-1α (Biolegend; #134306) on a BD LSRFortessa X-20. Data were analyzed using FlowJo software (Supp Fig. 1B). Cells were suspended in RPMI 1640 medium to a density of 1×10^7 cells per 200 μl. These cells were administered intravenously at a dose of 200 μl into four-week-old Kit^{W^{-sh}/W^{-sh}} mice.

Treatment of choroidal explants

Choroidal explants were obtained from 6-week-old mice. The choroidal explants were prepared according to a previously described procedure [22]. Briefly, mice eyes were dissected in a Petri dish containing Hank's balanced salt solution (HBSS; 02-0121-0500; VWR, QC, Canada). The eyes were dissected below the ora serrata to remove the lens and cornea and the neuroretina was carefully removed. The complexes formed by RPE-choroid-sclera were then collected, cut in 16 explant fragments, and

plated on Matrigel (BD biosciences) in 24-well plates. Choroidal explants were cultured at 37 °C in 5% CO₂ for 4 days in endothelial cell growth basal medium (EBM-2) supplemented with Microvascular Endothelial SingleQuots kit (EGM-2MV; respectively, CC-3156 and CC-4147; Lonza Bioscience, Basel, Switzerland). Explants were stimulated at day 5 with conditioned media of peritoneal mast cells activated with compound 48/80 or tryptase and incubated for 24 h. Images were taken before (time 0) and 24 h after stimulation. Quantification of sprouting area was performed using ImageJ software analysis.

Preparation of anti-CD31 antibody coated magnetic beads

Sheep anti-rat Dynabeads (DynaL Biotech) were washed three times with serum-free DMEM (Dulbecco's Modified Eagle's Medium; Invitrogen) and then incubated with rat anti-mouse CD31 monoclonal antibody MEC13.3 (BD Pharmingen) overnight at 4 °C. Following incubation, beads were washed three times with DMEM containing 10% FBS and resuspended in the same medium, and stored at 4 °C.

Isolation and culture of choroidal endothelial cells

Twelve eyes of 4-week-old pups (C57BL/6) were enucleated, and the RPE/Choroid/sclera complex was dissected under a stereoscopic microscope in cold DMEM. Each isolation used a litter of 6 pups, resulting in 12 RPE/Choroid/sclera complexes pooled together. These complexes were rinsed with DMEM, minced into small pieces in a tissue culture dish using sterile stainless steel surgical blades, and digested in 5 mL of collagenase type I (1 mg/mL) in serum-free DMEM for 45 min at 37 °C. After digestion, 10% FBS in DMEM was added to stop collagenase activity. The cells were then filtered through a double layer of sterile 40 mm nylon mesh (Fisher Scientific) and centrifuged at 500 x g for 10 min to settle the cells. Cells were washed twice with DMEM containing 10% FBS. The cells were resuspended in 1 mL DMEM with 10% FBS and incubated with sheep anti-rat magnetic beads precoated with anti-CD31 as described above. After affinity binding, magnetic beads were washed 6 times with DMEM with 10% FBS and bound cells in endothelial cell growth medium were plated into a single well of a 24-well plate pre-coated with 2 mg/mL of attachment factor (Life Technologies). Endothelial cells were grown in DMEM containing 10% FBS, 2 mM L-glutamine, 2 mM sodium pyruvate, 20 mM HEPES, 1% non-essential amino acids, 1% streptomycin/penicillin, 55 U/mL freshly added heparin (Sigma), and 100 mg/mL endothelial growth supplement (Sigma). Cells were incubated at 37 °C and 5% CO₂. Cells were progressively propagated in attachment factor-coated 60 mm dishes and used in early passages (3–5).

Scratch-wound assay

Confluent choroidal endothelial cells were grown in 6-well plates. Cells were starved 18 h in EBM-2 medium with 1% FBS. A horizontal wound was created using a sterile 200 μ l pipette tip. The cells were washed with EBM2 at 37 °C and incubated in PMC conditioned media or EBM-2 supplemented recombinant tryptase. Pictures of scratch wounds were taken before stimulation (time 0) and after 24 h. Migration % was calculated using ImageJ software.

Tubule formation assay

Choroidal endothelial cells were plated at a density of 30,000 cells/well in 96-well plates precoated with 50 μ L of growth factor-reduced Matrigel Matrix (Fisher Scientific, New Hampshire, USA) and cultured at 37 °C for 6 h in complete endothelial growth medium. Capillary-like tubes were observed under a light microscope. Images were obtained at 10X magnification. In each well, images were taken from four random fields. Tubes and branching point were counted.

RNA-seq sample preparation, sequencing, and analysis

Total RNA was extracted from the RPE/choroid/sclera complex of C57BL6 mice, including both CNV eyes 3 days post laser burn, and age-matched control eyes (no laser burn). RNA extraction was performed using RNeasy Mini Kit (QIAGEN) according to the manufacturer's protocol. RNA was quantified using Qubit (Thermo Scientific) and quality was assessed with the 2100 Bioanalyzer (Agilent Technologies). Transcriptome libraries were generated using the KAPA RNA HyperPrep (Roche) using a poly-A selection (Thermo Scientific). Sequencing was performed on the Illumina NextSeq500, obtaining around 25 M single-end 75 bp reads per sample. Sequences were trimmed for sequencing adapters and low-quality 3' bases using Trimmomatic (version 0.35) and aligned to the reference mouse genome version GRCm38 (gene annotation from Gencode version M23, based on Ensembl 98) using STAR version 2.7.1a. Gene expressions were obtained as read counts directly from the STAR output and also computed transcript-level expressions via RSEM, generating normalized values in transcripts per million (TPM) for these stranded RNA libraries. DESeq2 (version 1.22.2) was used to normalize gene read counts which allowed the hierarchical clustering of samples based on normalized log-transformed read counts. Principal component analysis was used to elucidate the two most significant components. Genes were sorted by adjusted p-values. Significant differentially expressed genes (DEGs) were defined as those with $\text{padj} < 0.05$.

Gene set enrichment analysis

The gene set enrichment analysis (GSEA) was carried out using GSEA software version 4.3.3, developed by the Broad Institute affiliated with both MIT and Harvard University. Selected gene sets were retrieved from the catalog of the Molecular Signature Database, which provides functionally annotated gene sets. For the analysis, the phenotype was subjected to 1,000 permutations, and the distinction between CNV versus control was used to define the phenotype label. Gene sets containing fewer than 15 or more than 500 genes were excluded. The analysis employed a weighted p2 statistic to identify significant genes, and a t-test was used as the metric to differentiate the classes.

GO pathway enrichment analysis

Gene ontology (GO) pathway enrichment analysis was performed using EnrichR Classification System. The top 100 up-regulated genes of CNV vs. control were used.

Collagen hybridizing peptide (CHP) binding

CHP binding was performed according to manufacturer's instructions. A solution containing 15 μ M of 5-FAP-CHP (3Helix) in PBS was heated at 80 °C for 5 min, and immediately cooled down to room temperature in an ice/water bath. The quenched CHP solution was quickly added onto the RPE/choroid complex. The RPE/choroid complex was incubated with the quenched CHP solution overnight at 4 °C and then washed. It was subsequently incubated with the TrueView Autofluorescence Quenching Kit (Vector; SP-8400-15) for 5 min at room temperature to reduce autofluorescence. The RPE/choroid complex was washed and flat-mounted onto glass slides with coverslips and Fluoro-Gel mounting medium (Electron Microscopy Sciences, Hatfield, PA).

Statistical analysis

Data are presented as mean \pm standard error of the mean (SEM). Student's t-test was used to compare two different groups. Additionally, a one-way analysis of variance (ANOVA) was conducted, followed by post hoc Holm-Sidak tests for comparison of means. A p-value < 0.05 was considered statistically significant.

Results

Mast cells promote choroidal endothelial cell sprouting angiogenesis and migration

To assess the proangiogenic role of mast cells, we used different models of angiogenesis ex-vivo and in vitro. First, we used a reproducible ex-vivo choroidal sprouting assay as a model of choroidal microvascular proliferation [22]. Mouse choroidal explants were treated with conditioned medium from compound 48/80-stimulated peritoneal mast cells for 24 h; peritoneal mast cells display

properties akin to connective tissue mast cells as found in choroid [23]. Compound 48/80 had negligible effect on choroidal sprouting likely because of the heterogeneous distribution of tissue-resident mast cells [24]. In contrast, treatment with conditioned medium from compound 48/80-stimulated peritoneal mast cells resulted

in a marked increase in choroidal sprouting (Fig. 1A, B). Compound 48/80-stimulated peritoneal mast cells also accelerated choroidal endothelial cell migration using a scratch assay (Fig. 1C, D) and enhanced tubulogenesis (Fig. 1E-G).

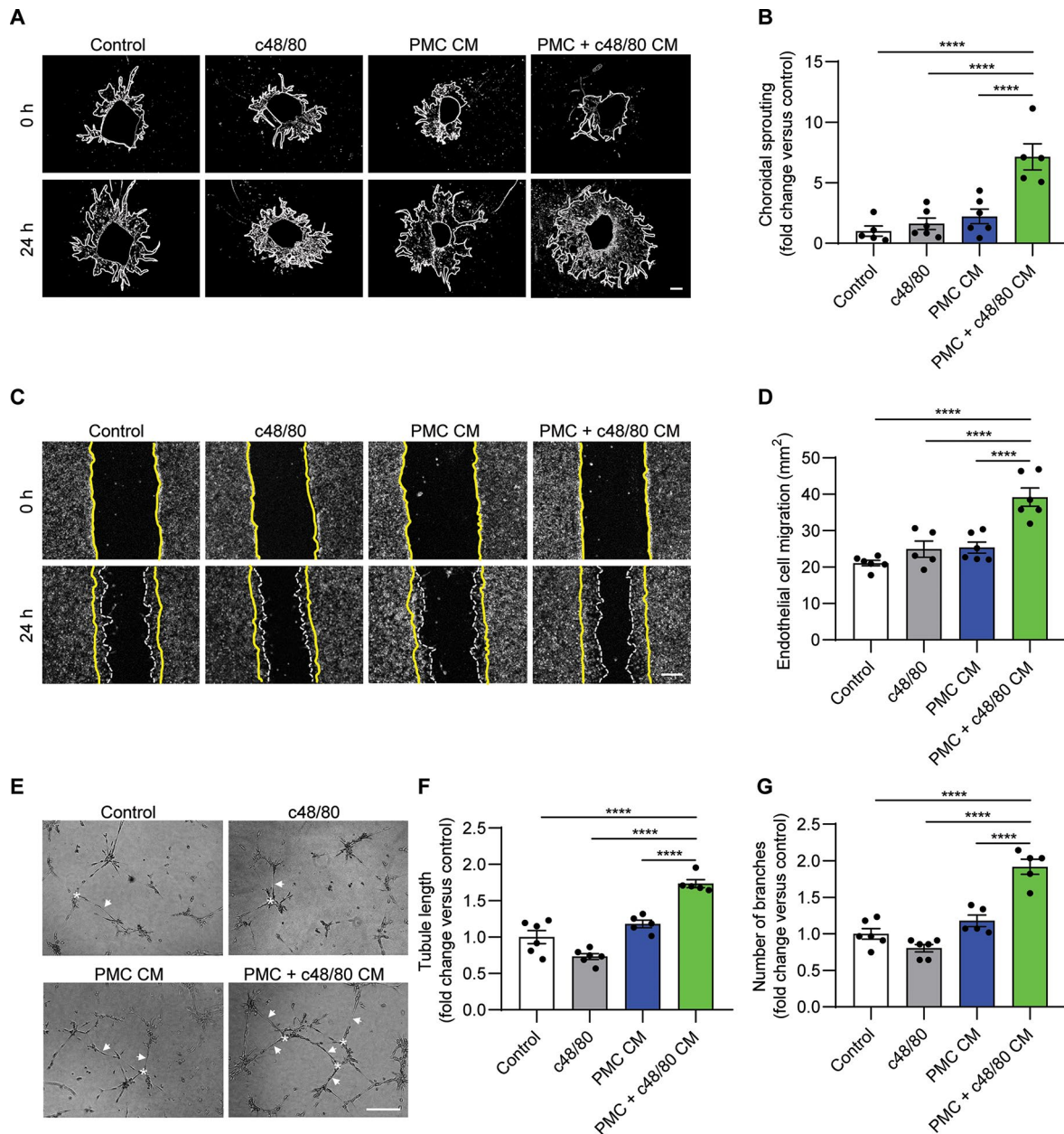


Fig. 1 Effects of mast cells on choroidal angiogenesis. **(A)** Representative image of choroidal explants cultured in the presence or absence of peritoneal mast cells (PMCs) treated or not with mast cell degranulator compound 48/80 (c48/80). Scale bar: 500 μ m. **(B)** Graph representing the quantification of sprouting surface area ($n=5-6$). Statistical analyses were performed using one-way ANOVA. $***p < 0.001$, $****p < 0.0001$. **(C)** Effects of mast cells on scratch wound migration after 24 h. Scale bar: 500 μ m. **(D)** Quantification of wound closure ($n=5-6$). Statistical analyses were performed using one-way ANOVA. $****p < 0.0001$. **(E)** Effects of mast cells on tubulogenesis as assessed in choroidal endothelial cells cultured in Matrigel. The arrows point to the tube-like structures and asterisks indicate branch points. Scale bar: 500 μ m. Quantification of the length of tubules **(F)** and the number of branches **(G)** ($n=5-6$). Statistical analyses were performed using one-way ANOVA. $****p < 0.0001$. The control group contains control media without any additives. c48/80 treatment: media containing c48/80. PMC CM: conditioned media derived from untreated PMCs. PMC + c48/80 CM: conditioned media derived from c48/80-stimulated PMCs

Mast cell deficiency (and stabilization) precludes choroidal neovascularization

Given the observed proangiogenic effects of mast cells on choroidal endothelial cells, both in vitro and ex vivo, we sought to determine their potential influence on CNV in vivo. Mast cells and their products are known to be present in sufficient quantities to exert substantial effects on physiological, immunological, and inflammatory responses in the choroid [25]. Following laser burn, an increase in the number of mast cells undergoing

degranulation (avidin D) was observed in choroidal flat mounts co-stained with lectins (vessel marker red; Fig. 2A). Mast cells were predominantly located at the CNV site (confirmed by z-stack analysis) on day 1 and furthermore on day 3 post-burn, with some granules observed diffusing above the RPE layer, and subsided by day 7 (Fig. 2A, Supp Fig. 2).

The role of mast cells was ascertained in choroidal neovascularization, using mast cell deficient-Kit^{W-sh/W-sh} mice. Following laser burn, we assessed the formation

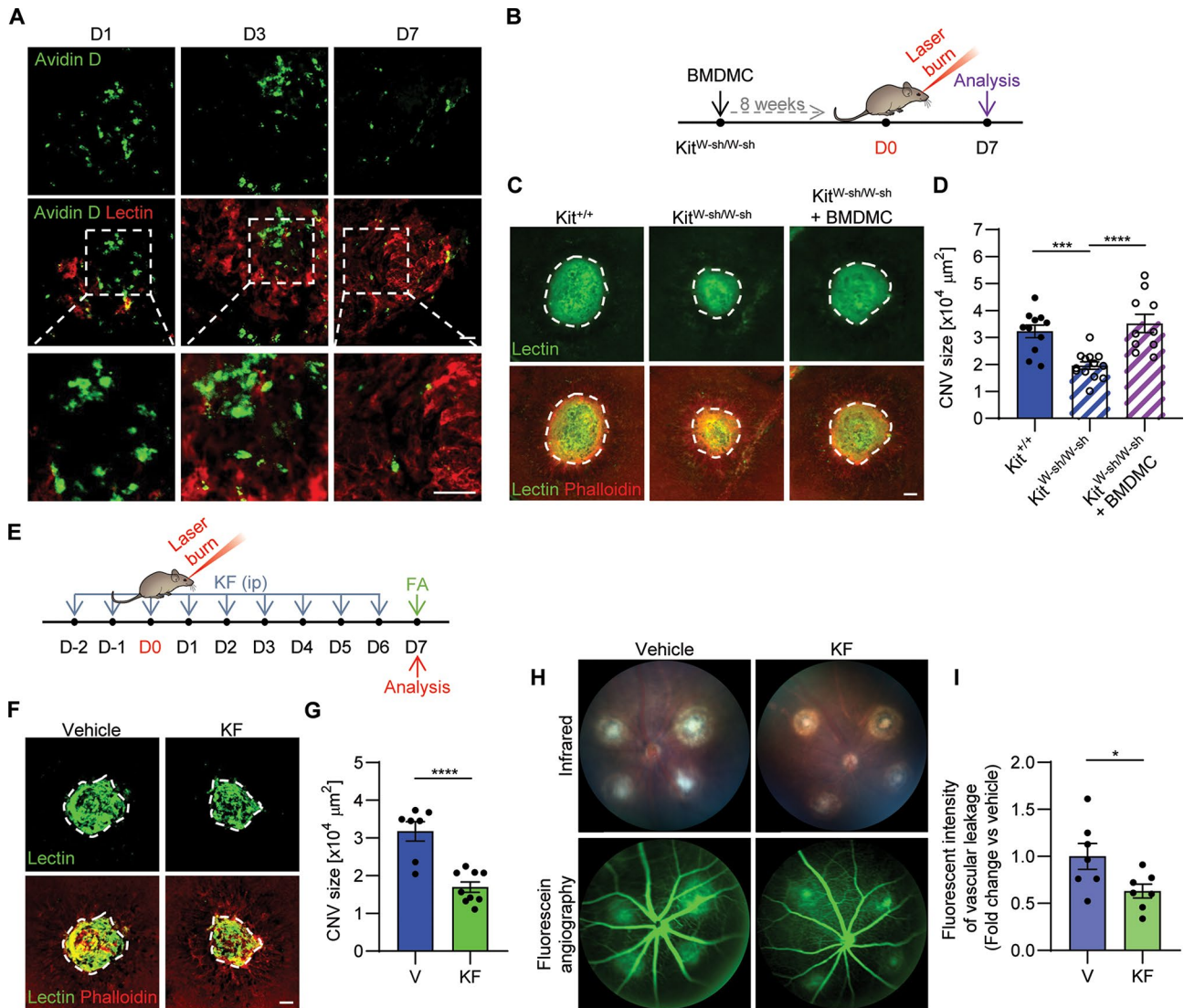


Fig. 2 Effects of mast cell deficiency on choroidal neovascularization. **(A)** RPE/choroid complex flat mounts illustrating the accumulation of mast cells (green) in the CNV lesion (red). Scale bar: 20 μm . **(B)** Timeline illustration of the laser-induced CNV model in mice. **(C)** Representative image of RPE/choroid complex flat mount staining with FITC lectin (green) and rhodamine phalloidin (red) in WT mice, Kit^{W-sh/W-sh} mice, and Kit^{W-sh/W-sh} mice reconstituted with BMDMCs at day 7 following laser burn. Scale bar: 50 μm . **(D)** Quantification of the CNV lesion size in RPE/choroid complex flat mounts ($n = 10-13$). Statistical analyses were performed using one-way ANOVA. *** $p < 0.001$, **** $p < 0.0001$. **(E)** Experimental timeline for ketotifen fumarate treatment in laser-induced CNV. **(F)** Representative image of RPE/choroid complex flat mounts after staining with FITC lectin (green) and rhodamine phalloidin (red) from mice at day 7 after receiving laser burn and treatment with vehicle or ketotifen fumarate (KF) at 25 mg/kg. Scale bar: 50 μm . **(G)** Quantification of the CNV lesion size in RPE/choroid complex flat mounts. Statistical analyses were performed using unpaired t-tests. **** $p < 0.0001$. $n = 7-9$. **(H)** Representative fundus fluorescein angiography images of mice receiving vehicle or KF 7 days after laser burn. **(I)** Quantification of vascular leakage. Statistical analyses were performed using Welch's t-test. * $p < 0.05$. $n = 7$

of new vessels using lectin (green) staining on RPE/choroidal flat mounts. *Kit*^{W-sh/W-sh} mice showed a marked decrease in CNV size on day 7 after laser injury (Fig. 2B-D); this decrease in CNV was prevented by mast cell replenishment upon systemic injection of BDMCs.

We further determined the role of mast cells by pharmacologically stabilizing them. Pre-treatment of mice subjected to laser burn with mast cell stabilizer ketotifen fumarate revealed a marked decrease in CNV size 7 days after laser impact (Fig. 2E-G). We also evaluated vascular permeability using fundus fluorescein angiography at the same interval. Ketotifen lessened the extent of vascular leakage at day 7 post-laser burn (Fig. 2H, I). Collectively, our findings using genetic and pharmacologic approaches reveal that mast cells contribute to the extent of CNV.

Mast cell tryptase promote pathological angiogenesis in the choroid

Next, we evaluated mast cell-derived tryptase as a critical pro-angiogenic agent in promoting CNV. Tryptase, a prominent protease present in mast cell granules, is a classic indicator of mast cell activation [26], and a potent angiogenic factor [27] upregulated in the choroid of AMD patients [28]. To explore the potential contribution of tryptase in choroidal angiogenesis, we treated choroidal endothelial cells with two different doses of mouse tryptase, mMCPT6 (100 and 1000 ng/mL), and subsequently performed migration and tube formation assays. mMCPT6 promoted endothelial cell migration (Fig. 3A, B) and tubulogenesis (Fig. 3C-E). Coherently, mMCPT6 increased choroidal sprouting *ex vivo* compared to control (Fig. 3F, G). As expected, we detected a substantial increase in avidin D and tryptase-positive mast cells located at the CNV lesion site on day 3 post-laser burn (Fig. 3H, I), corroborating with clinical observations in AMD [29]. To validate *in vivo* the proangiogenic role of tryptase, we found that the tryptase inhibitor, APC 366, significantly reduced CNV lesion size by day 7 post-laser burn (Fig. 3J-K).

Mast cells promote extracellular matrix (ECM) remodelling

Finally, to elucidate the cellular processes that are associated with mast cell activation, we conducted a comprehensive and unbiased transcriptomic analysis on the RPE/choroid complex 3 days after laser burn. Gene set enrichment analysis (GSEA) revealed a significant correlation in clusters of mast cell activation (normalized enrichment score [NES], 1.59; false discovery rate [FDRq], 0.005), collagen catabolism (NES, 1.57; FDRq, 0.007), and ECM organization (NES, 1.56; FDRq, 0.032) (Fig. 4A). Gene ontology (GO) enrichment analysis of the top upregulated genes in laser burns (relative to control) uncovered ECM remodeling and innate immune response pathways (Fig. 4B, C). Consistent with these observations,

increased CHP binding was observed in the choroidal tissue of submacular sections of individuals at high genetic risk for developing AMD and in those with AMD [29]. To assess if mast cells promote pathological collagen deposition and dysfunctional ECM synthesis in choroidal neovascularization, we used CHP to assess collagen turnover - an indicator of ECM remodelling; CHP is a short amino acid sequence that has a high affinity for denatured collagen, typically found in damaged or remodeling tissues, by triple helix hybridization [30]. Compared to wild-type animals CHP binding on day 7 post-laser burn to eyes was decreased in *Kit*^{W-sh/W-sh} mice and restored by mast cell reconstitution (Fig. 4D, E), indicative of a pivotal role for mast cells in collagen remodeling.

Discussion

Chronic inflammation is recognized as a key contributor in the development and progression of CNV. In this context, the choroid in AMD patients emerges as an inflammatory milieu where macrophages and mast cells become more abundant [21, 31]. Prior findings have provided evidence that activated mast cells can influence choroidal function, particularly by increasing vasodilation and vascular permeability [32]. Mast cells also induce angiogenesis and have been shown to be present around the Bruch's membrane in both the early and late stage of CNV [21]. In this regard, we reveal that following laser burn induction, there is a rapid activation and migration of tissue resident mast cells to the site of injury highlighting the potential of mast cells as early initiators in CNV pathogenesis. Furthermore, mast cells clearly promoted choroidal endothelial cell migration and vessel sprouting *ex vivo* in choroidal explants. The proangiogenic role of mast cells was revealed in experiments with mast cell-deficient *Kit*^{Wsh/W-sh} mice as well as using a pharmacologic stabilizer of mast cells, ketotifen fumarate. Importantly, when mast cells were reconstituted, the extent of CNV was readily exacerbated, although reconstituted mast cells were scarcely detected in the chorio-sclera of these mice. Interestingly, in the context of resistance against VEGF-based therapy, often seen in some AMD patients, mast cells have been identified to confer this resistance in tumorigenesis [33]. A high level of granzyme B immunoreactivity was observed in the choroid of AMD donor eyes [34], correlating with its role in enhancing choroidal angiogenesis [35]. Thus, mast cells should be considered an important therapeutic target in AMD subjects.

A key feature of our work applies to secreted factors from mast cells. A myriad of mediators such as histamines, lipid mediators, cytokines, and chemokines are released by mast cells upon activation. We clearly found that cell media from activated mast cells induced endothelial cell migration, tubulogenesis, and

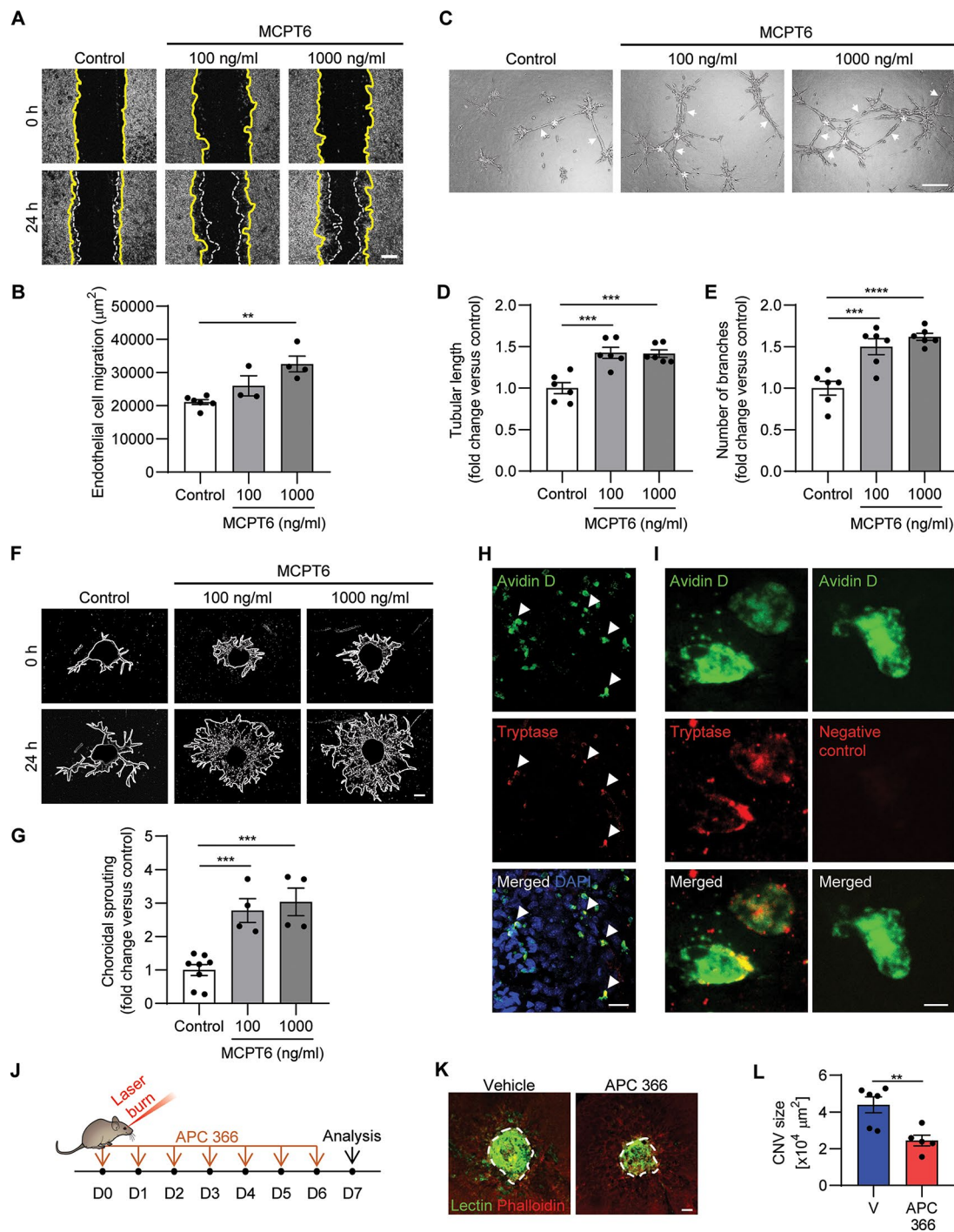


Fig. 3 Effects of tryptase on choroidal angiogenesis. **(A)** Effects of mouse tryptase (mMCPT6) at the indicated dose on scratch wound migration after 24 h. Scale bar: 500 μm . **(B)** Quantification of wound closure ($n=4-6$). Statistical analyses were performed using one-way ANOVA. $**p < 0.01$. **(C)** Effects of mMCPT6 on tubulogenesis using choroidal endothelial cells. The arrows indicate tube-like structures and asterisks mark the branch points. Scale bar: 500 μm . Quantification of **(D)** the length of tubules and **(E)** the number of branches ($n=6$). Statistical analyses were performed using one-way ANOVA. **(F)** Representative image of choroidal explants treated or not with mMCPT6. Scale bar: 500 μm . **(G)** Graph representing the quantification of sprouting surface area ($n=4-7$). Statistical analyses were performed using one-way ANOVA. **(H)** Representative images of avidin positive (green) mast cells expressing tryptase (red), indicated by arrowheads, 3 days following laser burn. Scale bar: 20 μm . **(I)** Representative high-magnification images of avidin-positive (green) mast cells expressing tryptase (red) 3 days following laser burn. Negative control indicates the staining without primary antibody. Scale bar: 5 μm . **(J)** Schematic illustration of the APC 366 treatment in laser-induced CNV mouse model. **(K)** Representative images of lectin-stained RPE/choroid flat mounts of mice treated with APC 366 or vehicle 7 days after laser burn. Scale bar: 50 μm . **(L)** The graph illustrates the quantification of the CNV lesion size in RPE/choroid complex flat mounts of mice treated with APC 366 or vehicle ($n=5, 6$). Statistical analyses were performed using unpaired t-test. $*p < 0.05$

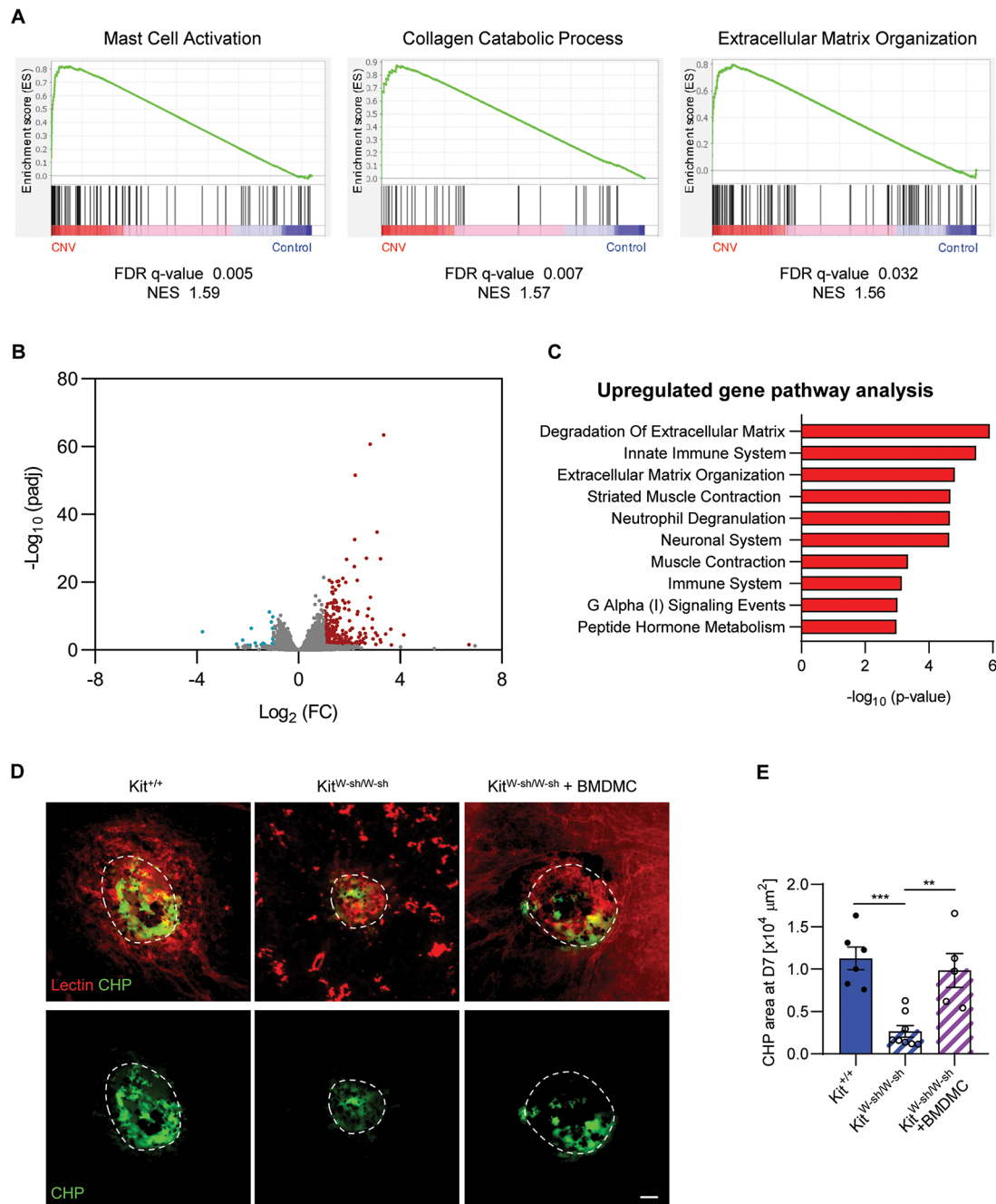


Fig. 4 Mast cells regulate collagen deposition in CNV. **(A)** GSEA pathway analysis of laser burn at day 3 versus control in RPE/choroid complex. **(B)** Volcano plot illustrating RNA-seq data from the choroid/RPE complex. Genes marked with red dots signify those with an adjusted p-value below 0.05 and a \log_2 fold change > 1 , while blue dots indicate genes with the same adjusted p-value and a \log_2 fold change < -1 . All remaining genes are depicted in gray. **(C)** Bar graph ranking the top 10 pathways based on their significance, as determined by gene ontology-term pathway enrichment analysis. **(D)** Representative images of RPE/choroid complex flat mounts stained with lectin (red) and collagen hybridizing peptide (CHP; green). Scale bar: 50 μm . **(E)** Quantification of CHP area. Statistical analyses were performed using one way ANOVA; $n = 5-8$. **** $p < 0.0001$, *** $p < 0.001$, ** $p < 0.01$

neovascularization, consistent with evidence of bioactive secreted factors. Relevantly, in individuals with a high genetic predisposition for AMD, mast cell protease levels were found to be augmented [29]. Among them, tryptase stood out with the most pronounced expression. As high-risk patients progressed to AMD, there was a steady

increase in tryptase levels [29]. Interestingly, tryptase has also been shown to be associated with pathological retinal neovascularization in other vasoproliferative retinopathies [36]. In support of these findings, we demonstrated that tryptase was able to promote choroidal endothelial cell migration and choroidal sprouting ex

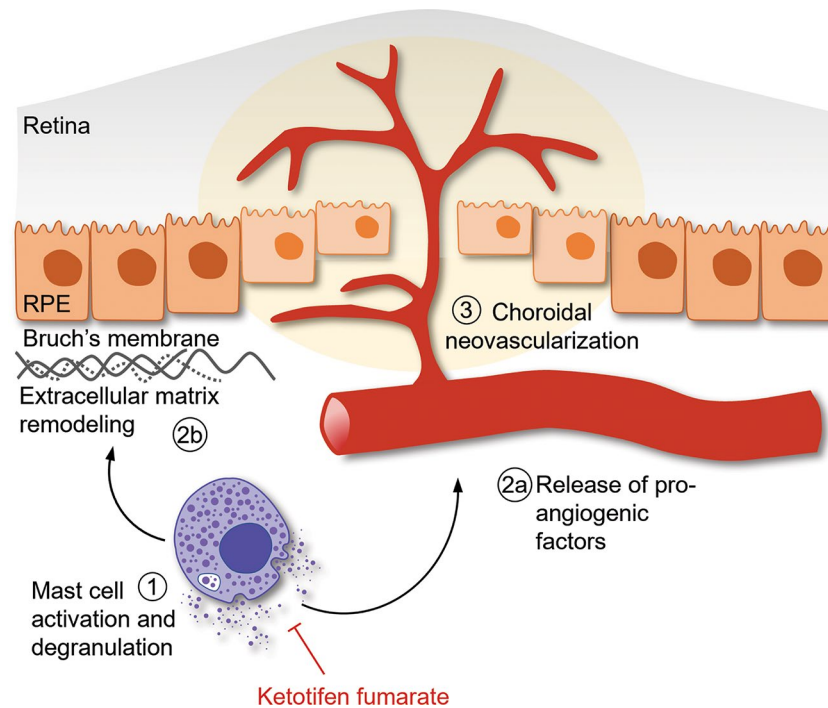


Fig. 5 A brief overview of how mast cells are implicated in choroidal neovascularization. Mast cell activation and degranulation results in ECM modelling and release of pro-angiogenic factors, and this can be alleviated using ketotifen fumarate

vivo; conversely, the selective mast cell tryptase inhibitor, APC 366 was able to reduce CNV lesion size in the laser impact model of AMD by reversing these endothelial proliferative effects in vivo. Collectively, these results suggest that suppression of mast cell activity should be considered as a possible therapeutic option to prevent pathological neovascularization in ocular disorders.

As part of the proliferative influence of mast cells on the endothelium, the CHP binding assay revealed that mast cells influence ECM composition. During angiogenesis, endothelial cells need to migrate across the ECM and the basement membrane, which pose as physical barriers. Matrix metalloproteases and other enzymes facilitate this process by degrading the ECM components, thereby allowing the migrating endothelial cells to invade the surrounding tissue and establish new vascular structures [37]. Moreover, the significance of ECM extends to the modulation of angiogenesis. Components of ECM can sequester a reservoir of growth factors such as VEGF and fibroblast growth factor (FGF) that can be released upon degradation of the ECM [38, 39]. Our findings showed that ECM remodeling is an important event during CNV and that mast cells promote pathological collagen deposition and dysfunctional ECM synthesis. Interestingly, genetic variants of the ECM have been associated with AMD [40]. Mast cells, known for their impact on tissue remodeling, can influence ECM directly through their proteolytic enzymes or by activating ECM-degrading enzymes such as matrix metalloproteinases

(MMPs) [41]. Bruch's membrane, a complex network located between the RPE and the choriocapillaris, is mainly composed of various types of collagens, fibronectin, laminin, and proteoglycans [42]. Therefore, choroidal mast cells can rupture Bruch's membrane and basement membrane, allowing the advancement of choroidal blood vessels toward the RPE and subretina; ultimately resulting in edema, hemorrhage, and fibrosis.

Limitations of this study applies to models of age-related macular degeneration. In this study we conducted our work on 10–12 week old mice to uncover the role of mast cells in CNV; the approach of using 10–12 week old mice was mostly based on practicality. Exploring the role of mast cells in older animals would provide a complementary dimension to this work, as more severe CNV is expected in older subjects [43]. Moreover, although the laser-burn induced CNV does not reflect the human condition of vasoproliferative AMD, it is the model most used in this context and thus contributes to the broader understanding of CNV pathogenesis and the development of novel treatment strategies for wet AMD.

In summary this study illustrates the profound impact of mast cells in promoting CNV and ECM remodeling; a model depicting mast cell role in CNV is shown in Fig. 5. Laser burn induces damage to the RPE leading to its degeneration, resulting in massive mast cell recruitment and activation. Local mast cell degranulation induces ocular inflammation and tryptase activation that cause damage to neighboring cells or an angiogenic response

resulting in choroidal pathological neovascularization. Pharmacological inhibition of mast cell degranulation or their secreted factors could pave the way for beneficial therapeutic interventions for AMD patients that complement current anti-VEGF treatments.

Abbreviations

| | |
|--------|--------------------------------------|
| AMD | Age-related macular degeneration |
| ANOVA | One-way analysis of variance |
| BMDMC | Bone marrow-derived mast cells |
| BSA | Bovine serum albumin |
| C48/80 | Compound 48/80 |
| CHP | Collagen hybridizing peptide |
| CNV | Choroidal neovascularization |
| DAPI | 4',6-Diamidino-2-phenylindole |
| DMEM | Dulbecco's Modified Eagle's Medium |
| EBM-2 | endothelial cell growth basal medium |
| ECM | Extracellular matrix |
| FBS | Fetal bovine serum |
| FGF | Fibroblast growth factor |
| GO | Gene ontology |
| GSEA | Gene set enrichment analysis |
| HBSS | Hank's balanced salt solution |
| KF | Ketotifen fumarate |
| MMPs | Matrix metalloproteinases |
| PBS | Phosphate-buffered saline |
| PFA | Paraformaldehyde |
| PMCs | Peritoneal mast cells |
| RPE | Retinal pigmented epithelium |
| RPMI | Roswell Park Memorial Institute |
| VEGF | Vascular endothelial growth factor |

Supplementary Information

The online version contains supplementary material available at <https://doi.org/10.1186/s12974-024-03229-x>.

Supplementary Material 1

Supplementary Material 2

Acknowledgements

This study was funded by the Canadian Institutes of Health Research (CIHR) 950-231837 (SC). RD is supported by Fonds de Recherche du Québec-Santé (FRQS). PA is supported by CIHR, FRQS, The Vision Health Research Network, and FROUM. SC holds a Canada Research Chair (Vision Science) and the Leopoldine Wolfe Chair in translational research in age-related macular degeneration.

Author contributions

R.D., P.A., and S.C. conceived the study. R.D. and P.A. designed and carried out experiments, analyzed the data, and wrote the manuscript. J.C.R. provided experimental support. J.C.R. and S.C. reviewed and edited the manuscript.

Data availability

No datasets were generated or analysed during the current study.

Declarations

Ethical approval

Animal studies were approved by the Maisonneuve Rosemont Hospital Animal Care Committee in accordance with the guidelines of the Canadian Council on Animal Care. Experiments were conducted in accordance with the Association for Research in Vision and Ophthalmology (ARVO) Statement for the Use of Animals in Ophthalmic and Visual Research.

Competing interests

The authors declare no competing interests.

Received: 6 May 2024 / Accepted: 10 September 2024

Published online: 01 October 2024

References

- Mitchell P, Liew G, Gopinath B, Wong TY. Age-related macular degeneration. *Lancet*. 2018;392(10153):1147–59.
- Wong WL, Su X, Li X, Cheung CM, Klein R, Cheng CY, et al. Global prevalence of age-related macular degeneration and disease burden projection for 2020 and 2040: a systematic review and meta-analysis. *Lancet Glob Health*. 2014;2(2):e106–16.
- Maberley D. Pegaptanib for neovascular age-related macular degeneration. *Issues Emerg Health Technol*. 2005(76):1–4.
- Grunwald JE, Daniel E, Huang J, Ying GS, Maguire MG, Toth CA, et al. Risk of geographic atrophy in the comparison of age-related macular degeneration treatments trials. *Ophthalmology*. 2014;121(1):150–61.
- Grunwald JE, Pistilli M, Daniel E, Ying GS, Pan W, Jaffe GJ, et al. Incidence and growth of Geographic Atrophy during 5 years of comparison of age-related Macular Degeneration treatments trials. *Ophthalmology*. 2017;124(1):97–104.
- Daniel E, Toth CA, Grunwald JE, Jaffe GJ, Martin DF, Fine SL, et al. Risk of scar in the comparison of age-related macular degeneration treatments trials. *Ophthalmology*. 2014;121(3):656–66.
- Galli SJ, Gaudenzio N, Tsai M. Mast cells in inflammation and disease: recent progress and ongoing concerns. *Annu Rev Immunol*. 2020;38:49–77.
- Grimbaldeston MA, Metz M, Yu M, Tsai M, Galli SJ. Effector and potential immunoregulatory roles of mast cells in IgE-associated acquired immune responses. *Curr Opin Immunol*. 2006;18(6):751–60.
- Moon TC, Befus AD, Kulka M. Mast cell mediators: their differential release and the secretory pathways involved. *Front Immunol*. 2014;5:569.
- Mukai K, Tsai M, Saito H, Galli SJ. Mast cells as sources of cytokines, chemokines, and growth factors. *Immunol Rev*. 2018;282(1):121–50.
- Theoharides TC, Alysandratos KD, Angelidou A, Delivanis DA, Sismanopoulos N, Zhang B, et al. Mast cells and inflammation. *Biochim Biophys Acta*. 2012;1822(1):21–33.
- Galli SJ, Tsai M. IgE and mast cells in allergic disease. *Nat Med*. 2012;18(5):693–704.
- Abraham SN, St John AL. Mast cell-orchestrated immunity to pathogens. *Nat Rev Immunol*. 2010;10(6):440–52.
- Varricchi G, de Paulis A, Marone G, Galli SJ. Future needs in mast cell Biology. *Int J Mol Sci*. 2019;20(18).
- Jones MK, Nair A, Gupta M. Mast cells in neurodegenerative disease. *Front Cell Neurosci*. 2019;13:171.
- Valent P, Akin C, Sperr WR, Horny HP, Arock M, Metcalfe DD, et al. New insights into the pathogenesis of mastocytosis: emerging concepts in diagnosis and therapy. *Annu Rev Pathol*. 2023;18:361–86.
- Gupta K, Harvima IT. Mast cell-neural interactions contribute to pain and itch. *Immunol Rev*. 2018;282(1):168–87.
- Lanzieri M, Cricchi M. Mast cells and vessels of the choroid of Albino Guinea Pigs during the Uveal Anaphylactic reaction. *Arch Ophthalmol*. 1965;74:367–70.
- Larsen G. The mast cells in the uveal tract of the eye and changes induced by hormones and avitaminosis-C. *Am J Ophthalmol*. 1959;47(1 Pt 2):509–19.
- McMenamin PG. The distribution of immune cells in the uveal tract of the normal eye. *Eye (Lond)*. 1997;11(Pt 2):183–93.
- Bhutto IA, McLeod DS, Jing T, Sunness JS, Seddon JM, Luttly GA. Increased choroidal mast cells and their degranulation in age-related macular degeneration. *Br J Ophthalmol*. 2016;100(5):720–6.
- Shao Z, Friedlander M, Hurst CG, Cui Z, Pei DT, Evans LP, et al. Choroid sprouting assay: an ex vivo model of microvascular angiogenesis. *PLoS ONE*. 2013;8(7):e69552.
- Akula S, Paivandy A, Fu Z, Thorpe M, Pejler G, Hellman L. How relevant Are bone marrow-derived mast cells (BMMCs) as models for tissue mast cells? A comparative transcriptome analysis of BMMCs and peritoneal mast cells. *Cells*. 2020;9(9).
- Zaitoun IS, Song YS, Zaitoun HB, Sorenson CM, Sheibani N. Assessment of Choroidal Vasculature and Innate Immune cells in the eyes of albino and pigmented mice. *Cells*. 2022;11(20).
- Godfrey WA. Characterization of the choroidal mast cell. *Trans Am Ophthalmol Soc*. 1987;85:557–99.

26. Schwartz LB, Metcalfe DD, Miller JS, Earl H, Sullivan T. Tryptase levels as an indicator of mast-cell activation in systemic anaphylaxis and mastocytosis. *N Engl J Med*. 1987;316(26):1622–6.
27. Blair RJ, Meng H, Marchese MJ, Ren S, Schwartz LB, Tonnesen MG, et al. Human mast cells stimulate vascular tube formation. Tryptase is a novel, potent angiogenic factor. *J Clin Invest*. 1997;99(11):2691–700.
28. McLeod DS, Bhutto I, Edwards MM, Gedam M, Baldeosingh R, Luty GA. Mast cell-derived tryptase in Geographic Atrophy. *Invest Ophthalmol Vis Sci*. 2017;58(13):5887–96.
29. McHarg S, Booth L, Perveen R, Riba Garcia I, Brace N, Bayatti N, et al. Mast cell infiltration of the choroid and protease release are early events in age-related macular degeneration associated with genetic risk at both chromosomes 1q32 and 10q26. *Proc Natl Acad Sci U S A*. 2022;119(20):e2118510119.
30. Li Y, Yu SM. Targeting and mimicking collagens via triple helical peptide assembly. *Curr Opin Chem Biol*. 2013;17(6):968–75.
31. McLeod DS, Bhutto I, Edwards MM, Silver RE, Seddon JM, Luty GA. Distribution and quantification of Choroidal macrophages in human eyes with age-related Macular Degeneration. *Invest Ophthalmol Vis Sci*. 2016;57(14):5843–55.
32. Bousquet E, Zhao M, Thillaye-Goldenberg B, Lorena V, Castaneda B, Naud MC, et al. Choroidal mast cells in retinal pathology: a potential target for intervention. *Am J Pathol*. 2015;185(8):2083–95.
33. Wroblewski M, Bauer R, Cubas Cordova M, Udonta F, Ben-Batalla I, Legler K, et al. Mast cells decrease efficacy of anti-angiogenic therapy by secreting matrix-degrading granzyme B. *Nat Commun*. 2017;8(1):269.
34. Matsubara JA, Tian Y, Cui JZ, Zeglinski MR, Hiroyasu S, Turner CT, et al. Retinal distribution and extracellular activity of Granzyme B: a serine protease that degrades retinal pigment epithelial tight junctions and Extracellular Matrix proteins. *Front Immunol*. 2020;11:574.
35. Obasanmi G, Uppal M, Cui JZ, Xi J, Ju MJ, Song J et al. Granzyme B degrades extracellular matrix and promotes inflammation and choroidal neovascularization. *Angiogenesis*. 2024;27(3):351–73.
36. Matsuda K, Okamoto N, Kondo M, Arkwright PD, Karasawa K, Ishizaka S, et al. Mast cell hyperactivity underpins the development of oxygen-induced retinopathy. *J Clin Invest*. 2017;127(11):3987–4000.
37. Kalluri R. Basement membranes: structure, assembly and role in tumour angiogenesis. *Nat Rev Cancer*. 2003;3(6):422–33.
38. Hynes RO. The extracellular matrix: not just pretty fibrils. *Science*. 2009;326(5957):1216–9.
39. Kessenbrock K, Plaks V, Werb Z. Matrix metalloproteinases: regulators of the tumor microenvironment. *Cell*. 2010;141(1):52–67.
40. Fritsche LG, Igl W, Bailey JN, Grassmann F, Sengupta S, Bragg-Gresham JL, et al. A large genome-wide association study of age-related macular degeneration highlights contributions of rare and common variants. *Nat Genet*. 2016;48(2):134–43.
41. Kovanen PT. Mast cells and degradation of pericellular and extracellular matrices: potential contributions to erosion, rupture and intraplaque haemorrhage of atherosclerotic plaques. *Biochem Soc Trans*. 2007;35(Pt 5):857–61.
42. Bhutto I, Luty G. Understanding age-related macular degeneration (AMD): relationships between the photoreceptor/retinal pigment epithelium/Bruch's membrane/choriocapillaris complex. *Mol Aspects Med*. 2012;33(4):295–317.
43. Espinosa-Heidmann DG, Suner I, Hernandez EP, Frazier WD, Csaky KG, Cousins SW. Age as an independent risk factor for severity of experimental choroidal neovascularization. *Invest Ophthalmol Vis Sci*. 2002;43(5):1567–73.

Publisher's note

Springer Nature remains neutral with regard to jurisdictional claims in published maps and institutional affiliations.